Aurantio-obtusin regulates lipogenesis and ferroptosis of liver cancer cells through inhibiting SCD1 and sensitizing RSL3

WEN LIU[1,2], JUN DENG[2], XIAO-JUN TAO[3], YA PENG[2], XIANG-DING CHEN[1], XIAO-CHAO QU[1], HONG-WEN DENG[4] and LI-JUN TAN[1]

[1]Laboratory of Molecular and Statistical Genetics, College of Life Sciences, Hunan Normal University, Changsha, Hunan 410081, P.R. China; [2]Department of Pharmacy, Hunan Provincial People's Hospital (The First Affiliated Hospital of Hunan Normal University), Changsha, Hunan 410000, P.R. China; [3]Key Laboratory of Study and Discovery of Small Targeted Molecules of Hunan Province, School of Medicine, Hunan Normal University, Changsha, Hunan 410013, P.R. China; [4]Tulane Center of Biomedical Informatics and Genomics, Deming Department of Medicine, Tulane University School of Medicine, New Orleans, LA 70112, USA

Received March 5, 2024; Accepted July 15, 2024

DOI: 10.3892/ijo.2024.5680

Abstract. Ferroptosis, characterized by iron-mediated non-apoptotic cell death and alterations in lipid redox metabolism, has emerged as a critical process implicated in various cellular functions, including cancer. Aurantio-obtusin (AO), a bioactive compound derived from Cassiae semen (the dried mature seeds of *Cassie obtusifolia* L. or *Cassia toral* L.), has anti-hyperlipidemic and antioxidant properties; however, to the best of our knowledge, the effect of AO on liver cancer cells remains unclear. The Cell Counting Kit-8, EdU staining and migration assays were employed to assess the anti-liver cancer activity of AO. Intracellular levels of glutathione peroxidase 4 protein and lipid peroxidation were measured as indicators of ferroptotic status. Immunohistochemical analyses, bioinformatics analyses and western blotting were conducted to evaluate the potential of stearoyl-CoA desaturase 1 (SCD1) in combination with ferroptosis inducers for the personalized treatment of liver cancer. The present study revealed that AO significantly inhibited the proliferation of liver cancer cells *in vitro* and *in vivo*. Mechanistically, AO inhibited AKT/mammalian target of rapamycin (mTOR) signaling, suppressed sterol regulatory element-binding protein 1 (SREBP1) expression, and downregulated fatty acid synthase expression, thereby inhibiting *de novo* fatty acid synthesis. Further investigations demonstrated that AO suppressed glutathione peroxidase 4 protein expression through the nuclear factor erythroid 2-related factor 2/heme oxygenase-1 pathway, induced ferroptosis in liver cancer cells, and simultaneously inhibited lipogenesis by suppressing SCD1 expression through the AKT/mTOR/SREBP1 pathway. Consequently, this increased the sensitivity of liver cancer cells to the ferroptosis inducer RSL3. Additionally, the enhanced effects of AO and RSL3, which resulted in significant tumor suppression, were confirmed in a xenograft mouse model. In conclusion, the present study demonstrated that AO induced ferroptosis, downregulated the expression of SCD1 and enhanced the sensitivity of liver cancer cells to the ferroptosis inducer RSL3. The synergistic use of AO and a ferroptosis inducer may have promising therapeutic effects in liver cancer cells.

Correspondence to: Dr Li-Jun Tan, Laboratory of Molecular and Statistical Genetics, College of Life Sciences, Hunan Normal University, 36 Lushan Street, Changsha, Hunan 410081, P.R. China
E-mail: ljtan@hunnu.edu.cn

Abbreviations: AO, aurantio-obtusin; mTOR, mammalian target of rapamycin; GPX4, glutathione peroxidase 4; SCD1, stearoyl-CoA desaturase1; SREBP1, sterol regulatory element-binding protein 1; FASN, fatty acid synthase; GSH, glutathione; MUFAs, monounsaturated fatty acids; Nrf2, nuclear factor erythroid 2-related factor 2; HO-1, heme oxygenase-1; Fer-1, ferrostatin-1; FBS, fetal bovine serum; LPO, lipid peroxide; PA, palmitic acid; AMPK, AMP-activated protein kinase; NAFLD, non-alcoholic fatty liver disease; TCGA, The Cancer Gene Atlas

Key words: liver cancer, AO, SCD1, GPX4, ferroptosis

Introduction

Liver cancer is one of the most common types of primary cancer and is among the leading causes of cancer-related deaths worldwide. In addition, it is associated with ~110,000 deaths each year in China (1,2). After staging assessments, only 20% of patients with early-stage liver cancer qualify for potentially curative treatments, such as liver resection, transplantation and local ablation (3). By contrast, the majority of patients with liver cancer, particularly those in the advanced stages, receive palliative or symptomatic care, resulting in a 3-year survival rate of <30% with most patients not surviving past 3 months (4). Accumulated clinical and epidemiological research has demonstrated that non-alcoholic fatty liver disease (NAFLD) is an independent risk factor for liver cancer that has emerged as a major cause due to its rapidly growing incidence (5-7). These findings indicate that altered lipid metabolism may serve a critical role in liver cancer, and that the identification of novel agents to treat liver cancer is urgently needed.

Dysregulation of lipid metabolism occurs in both cancer tissues and cancer cells (8). A growing body of evidence has indicated that activation of the fatty acid synthesis pathway may serve a pivotal role in cancer initiation (9,10). Previous studies have consistently linked abnormal lipogenesis to cancer development, since uncontrolled lipogenesis is vital for providing cancer cells with an abundant supply of lipid components and facilitating their uncontrolled proliferation (11,12). Notably, increased lipid biosynthesis promotes cancer progression in liver cancer cells. Furthermore, inhibition of fatty acid synthase (FASN), a key enzyme governing lipogenesis, is considered a promising strategy for blocking the proliferation of human liver cancer cells (13). Previous investigations have indicated that sterol regulatory element-binding protein 1 (SREBP1), a well-established transcriptional master regulator involved in lipogenesis, contributes to the progression of liver cancer by stimulating cancer cell proliferation and metastasis (14-16). Notably, mammalian target of rapamycin (mTOR) is crucial for SREBP1 regulation (17). Inhibition of the mTOR/SREBP1 pathway has been shown to negatively affect lipogenesis (18,19). Additionally, heightened lipogenesis can affect the sensitivity of liver cancer cells to anticancer drugs (20). These findings indicate the crucial role of elevated lipogenesis as a driving force of liver cancer progression; however, the precise molecular mechanisms underlying increased lipogenesis in liver cancer remain to be elucidated.

Ferroptosis is a novel form of cell death, and depletion of glutathione (GSH), inactivation of GSH peroxidase 4 (GPX4), and accumulation of cellular iron and lipid reactive oxygen species (ROS) are the typical molecular events of this type of cell death (21). Ferroptosis serves an important role in the development of liver cancer (22), and the precise targeting of tumor cells to induce ferroptosis is a new approach for the treatment of this type of cancer. In addition, sorafenib resistance in liver cancer has been reported to be associated with ferroptosis (23) through the upregulation of antioxidant pathways [such as nuclear factor erythroid 2-related factor 2 (Nrf2)], altered GPX4 expression, increased ferritin and decreased free iron levels, and reduced polyunsaturated fatty acids (24-27).

Stearoyl-CoA desaturase 1 (SCD1), which is regulated by SREBP1, is a critical modulator of fatty acid metabolism (28). SCD1 desaturates palmitoyl-CoA or stearoyl-CoA to form palmitoleic acid and oleic acid, respectively (28). Upregulation of SCD1 can increase the synthesis of monounsaturated fatty acids (MUFAs) and protect cancer cells against ferroptosis (29,30). Moreover, SCD1 has been reported to be significantly upregulated in liver cancer cells (28,31,32), and SCD1 expression has been linked to a poor prognosis in several types of cancer, such as hepatocellular, gastric and ovarian cancer (29,31,33,34). RSL3 is a small-molecule compound that inhibits the activity of GPX4, promoting lipid peroxidation and triggering ferroptosis in susceptible cells (35). Inhibition of SCD1 has been shown to promote RSL3-induced ferroptosis in colorectal cancer cells (36). Collectively, these studies suggest that a combination of SCD1 inhibitors and ferroptosis inducers may exert promising therapeutic effects in cancer treatment.

Cassiae semen, which refers to the dried mature seeds of *Cassie obtusifolia* L. or *Cassia toral* L., and is commonly known as sicklepod, belongs to the Leguminosae family. This plant product is widely cultivated in Korea and China, and is easily grown and often used as a popular roasted tea (37). Cassiae semen has a longstanding tradition of being used as a herbal remedy for liver and eye-related disorders. Aurantio-obtusin (AO), the primary bioactive compound derived from Cassiae semen, is characterized by its unique anthraquinone structure (38). Notably, the backbone of anthraquinones is a pivotal structural blocker in the development of anticancer drugs (39). AO exhibits a wide range of pharmacological effects, including neuroprotective, hepatoprotective, anti-hyperlipidemic, antioxidant, antimicrobial and anti-allergic activities (37,38,40,41). In addition, AO has been shown to reduce SREBP1c, FASN and SCD1 levels in the white adipose tissue of obese mice (40); however, in the brown adipose tissue of obese mice, AO can significantly enhance mitochondrial metabolism and uncoupling protein 1 expression by activating PPARα (42). Additionally, AO may attenuate NAFLD by inhibiting *de novo* lipid synthesis, which is regulated by SREBP1, and by promoting autophagy flux to alleviate liver steatosis in a mouse model of NAFLD (42). Several studies have demonstrated a close link between the inhibition of lipogenesis and the induction of ferroptosis in overcoming chemotherapy resistance (20,36). However, few investigations have focused on the relationship between AO and ferroptosis, which could represent a novel approach to sensitizing tumors to chemotherapy (24,26,43). Given that AO exhibits strong lipogenesis-inhibiting capabilities, the present study hypothesized that the regulatory effects of AO on lipogenesis may serve a crucial role in liver tumor growth, survival and sensitivity to ferroptosis.

The present study explored the anticancer activities of AO, when administered either alone or in combination with the ferroptosis inducer RSL3, and the underlying mechanisms were investigated. The present findings may pioneer the synergistic use of AO with a ferroptosis inducer as an innovative strategy for inhibiting liver cancer cell proliferation, with potential implications for future clinical use.

Materials and methods

Reagents. AO, RSL3 and ferrostatin-1 (Fer-1, ferroptosis inhibitor) were purchased from Shanghai Macklin Biochemical Co., Ltd. A939572 (SCD1 inhibitor) was purchased from Sigma-Aldrich; Merck KGaA. Palmitic acid (PA) was obtained from Beijing Solarbio Science & Technology Co., Ltd. (cat. no. SP8060). MK2206 (AKT inhibitor; cat. no. S1078) was purchased from Selleck Chemicals. Anti-GAPDH (cat. no. 2118; 1:1,000), anti-phosphorylated (p)-AKT (cat. no. 4060; 1:1,000), anti-AKT (cat. no. 9272; 1:1,000), anti-AMP-activated protein kinase (AMPK)α (cat. no. 2532; 1:1,000), anti-p-AMPKα (cat. no. 50081; 1:1,000), anti-p-mTOR (cat. no. 5536; 1:1,000), anti-mTOR (cat. no. 2983; 1:1,000), anti-FASN (cat. no. 3180; 1:1,000), anti-Nrf2 (cat. no. 12721; 1:1,000), anti-heme oxygenase 1 (HO-1; cat. no. 43966; 1:1,000), anti-GPX4 (cat. no. 52455; 1:1,000) and anti-SCD1 (cat. no. 2794; 1:1,000) antibodies were purchased from Cell Signaling Technology, Inc., and anti-SREBP1 (cat. no. sc-365513; 1:500) was purchased from Santa Cruz Biotechnology, Inc. All other reagents used in the experiments met or exceeded analytical grade standards. The clinical liver cancer sample data used in the present study

were obtained from The Cancer Gene Atlas (TCGA) project available in the ULCAN database (https://ualcan.path.uab.edu) (44). A total of 371 primary liver tumor samples and 50 normal liver tissue samples from healthy controls were used in the analysis. Pearson correlation analysis was used to assess the correlations between samples.

Specimen collection and patient information. Liver cancer specimens and adjacent normal tissues were collected from patients who underwent surgical resection at Hunan Provincial People's Hospital (Changsha, China). The present study was approved by The Ethics Committee of Hunan Provincial People's Hospital [approval no. (2023)-178]. A total of 15 patients were included in the study. The average age of the patients was 61.7 years (age range, 53-71 years), and the cohort consisted of nine men and six women. The normal specimens used in the present study were adjacent healthy tissues from the same patients from whom the liver cancer specimens were obtained.

Cell lines and culture conditions. Human liver cancer cells lines SK-Hep1 and HepG2 cells were provided by the Medical College of Hunan Normal University (Changsha, China). SK-Hep1 cells were maintained in basic RPMI 1640 medium (Gibco; Thermo Fisher Scientific, Inc.), whereas HepG2 cells were cultured in DMEM (Gibco; Thermo Fisher Scientific, Inc.). Both culture media were supplemented with 10% fetal bovine serum (FBS; Suzhou ExCell Biology, Inc.) and 1% penicillin-streptomycin (Gibco; Thermo Fisher Scientific, Inc.). The cell cultures were incubated at 37˚C in a humidified atmosphere containing 5% CO_2.

Cell viability and clonogenic assays. Cell viability was assessed using the Cell Counting Kit (CCK)-8 Cell Proliferation and Cytotoxicity Assay Kit (cat. no. CA1210; Beijing Solarbio Science & Technology Co., Ltd.). Briefly, cells were seeded at a density of $8x10^3$ cells/well in 96-well culture plates and cultured in medium containing 10% FBS at 37˚C. After 24 h, the cells were treated with 10-600 μM AO, 5-800 μM PA or 0.05-8 nM RSL3, for 48 h at 37˚C. For the combined treatment, the cells were treated with AO (50 μM), PA (SK-Hep1: 10 μM, HepG2: 100 μM), MK2206 (1 μM), A9 (8 μM), Fer-1 (5 nM), RSL3 (SK-Hep1: 0.01 nM, HepG2: 1 nM) or their combination at the indicated concentrations for 48 h at 37˚C. A 10% CCK-8 solution was prepared in medium and added to each well, and the plates were incubated for a further 1.5 h at 37˚C. Finally, the absorbance was measured at 450 nm using a microplate reader (Synergy HTX; BioTek; Agilent Technologies, Inc.). Dose-response curves were generated and the half-maximal inhibitory concentration was determined using SPSS (version 16.0; SPSS, Inc.).

Clonogenic survival was assessed by determining the colony-forming capacity of cells. Briefly, $8x10^3$ cells were seeded into 24-well dishes in 0.5 ml medium. After 24 h, cells were treated with varying concentrations of AO (0, 100 and 200 μM) daily for 7 consecutive days. For the combination therapy, the cells were treated with AO (0, 100 and 200 μM), PA (100 μM for HepG2 cells) or treated with RSL3 (0, 0.01 and 0.02 nM for SK-Hep1 cells and 0, 1 and 2 nM for HepG2 cells), A9 (8 μM for SK-Hep1), AO (50 μM for SK-Hep1) daily for 7 consecutive days in 1 ml medium containing 10% FBS at 37˚C. Subsequently, cells were fixed with 10% formaldehyde (0.5 ml) for 30 min at room temperature and stained with 0.1% crystal violet for 2 h at room temperature. Colonies consisting of >50 cells were detected. Using a microplate reader (BioTek; Agilent Technologies, Inc.), absorbance was measured at 550 nm using the area scanning function to quantify the number of cell colonies.

EdU staining. An EdU Cell Proliferation Kit with Alexa Fluor 488 (cat. no. KGA331; Nanjing KeyGen Biotech Co., Ltd.) was used to detect proliferating cells according to the manufacturer's instructions. Briefly, cells were seeded at a density of $8x10^3$ cells/well in 96-well culture plates and cultured in medium containing 10% FBS at 37˚C. After 24 h, the cells were treated with AO (0, 100 and 200 μM) for 24 h at 37˚C. For the combination therapy, the cells were treated with A9 (8 μM), RSL3 (SK-Hep1: 0.01 nM, HepG2: 1 nM), AO (50 μM) or their combination at the indicated concentrations for 24 h at 37˚C. Then pre-warmed EdU working solution was added to the treated cells for EdU labeling and was incubated for 2 h at 37˚C. After incubation, the medium was removed and 50 μl 4% neutral paraformaldehyde was added to each well, followed by incubation at room temperature for 30 min. The fixing solution was then removed and 50 μl 2 mg/ml glycine solution was added to each well, and incubated at room temperature for 5 min. Subsequently, cells were washed twice with 0.1 ml/well 3% bovine serum albumin (cat. no. ST2254-5g; Beyotime Institute of Biotechnology) in PBS, followed by incubation at room temperature for 20 min. Click-iT reaction solution (100 μl) was then added to each well and incubated at room temperature for 30 min in the dark. Finally, 0.1 ml 1X Hoechst 33342 solution was added to each well, followed by incubation at room temperature for 15-30 min in the dark. After staining, images were captured using an Olympus BX51 fluorescence microscope (Olympus Corporation).

Lipid peroxidation. Lipid peroxidation was assessed using the Lipid Peroxide (LPO) Content Assay Kit (cat. no. BC5245; Beijing Solarbio Science & Technology Co., Ltd.), according to the manufacturer's instructions. Briefly, cells were seeded at a density of $5x10^6$ cells/100-mm culture dish and were incubated at 37˚C in a 5% CO_2 incubator. The next day, cells were treated with varying concentrations of AO (50, 100 and 200 μM) for 24 h at 37˚C. For the combined treatment, the cells were treated with A9 (8 μM), RSL3 (SK-Hep1: 0.01 nM, HepG2: 1 nM), AO (50 μM), or their combination at the indicated concentrations for 24 h at 37˚C. The cells (~$5x10^7$) were then harvested and treated with the extraction solution. Subsequently, cells were disrupted using ultrasonic waves in an ice bath (frequency, 20 kHZ; power, 200 W; ultrasonication, 3 sec; interval, 7 sec; total time, 3 min) and centrifuged at 8,000 x g and 4˚C for 10 min. The resulting supernatant was collected, and reagent solutions were added according to the manufacturer's instructions. Finally, the absorbance of each sample was measured at 532 nm, then at 600 nm.

Small interfering RNA (siRNA) transfection. Cells were transfected with commercially available SCD1 siRNAs (siSCD1), with the following sequences: siSCD1-1, sense 5'-GAGACGAUG CCCCUCUACUUGG-3', antisense 5'-CCA AGUAGAGGG

GCAUCGUCUC-3'; siSCD1-2, sense 5'-GGAGAAACAUCA UCCUUAUUU-3', antisense 5'-AAAUAAGGAUGAUGUUUC UCC-3', or with the following negative control siRNA: sense 5'-UUCUCCGAACGUGUCACGUTT-3', anti-sense 5'-ACG UGACACGUUCGGAGAATT-3' (all from Guangzhou RiboBio Co., Ltd.) using the transfection reagent Lipofectamine® 2000 (Invitrogen; Thermo Fisher Scientific, Inc.). Briefly, cells were seeded in 6-well plates at a density of $3x10^5$ cells/dish. When cells reached 30-50% confluence, they were transfected with 50 nM siSCD1 or 50 nM negative control siRNA using Lipofectamine 2000 in the presence of 1% penicillin-streptomycin and 10% FBS, for 6 h at 37˚C. After washing with PBS, the medium was replaced with RPMI-1640 or DMEM. After 36 h, cell proteins were harvested and the effectiveness of silencing was confirmed through western blot analysis.

Western blotting. Cells were seeded at a density of $5x10^5$ cells/well in 6-well culture plates and cultured in medium containing 10% FBS at 37˚C. After 24 h, the cells were treated with AO (100 μM) for 6, 12 or 24 h, or with AO (50, 100 and 200 μM) for 24 h at 37˚C. For the combined treatment, the cells were treated with AO (50 μM), MK2206 (1 μM), A9 (8 μM), RSL3 (0.01 nM for SK-Hep1, 1 nM for HepG2), or their combination at the indicated concentrations for 24 h at 37˚C. Cells were then suspended in ice-cold RIPA buffer (Beyotime Institute of Biotechnology) containing 2% protease and phosphatase inhibitor cocktail (Beyotime Institute of Biotechnology). The protein concentration of lysates was then measured using the BCA assay. Homogenates containing 20 μg total protein were separated by SDS-PAGE on gradient gels (10-15%) and were transferred to polyvinylidene fluoride membranes (MilliporeSigma). The blocking reagent used was 5% non-fat milk at room temperature for 1 h, followed by three washes with TBS-0.1% Tween. The membranes were blotted with specific primary antibodies overnight at 4˚C with shaking, followed by incubation with HRP-conjugated secondary anti-rabbit or anti-mouse antibodies (cat. nos. L3032 and L3012; 1:10,000; Signalway Antibody LLC) for 1 h at room temperature. The membranes were then visualized using enhanced chemiluminescence (cat. no. PMK0448; Wuhan Pumoke Biotechnology Co., Ltd.) and a Gel Doc 2000 system (Bio-Rad Laboratories, Inc.). Band intensities were semi-quantified using ImageJ version 1.8.0 software (National Institutes of Health).

Transwell migration assay. Cell migration was assessed using Transwell plates (24-well insert; pore size, 8 μm; Corning, Inc.). Approximately $4x10^4$ cells/well in 200 μl serum-free medium were seeded into the upper chambers, while 700 μl medium supplemented with 20% FBS served as a chemoattractant in the lower chamber. The next day, cells were treated with AO (100 and 200 μM) for 24 h at 37˚C in 5% CO_2, the medium in the upper chamber was aspirated and the cells were fixed with 4% paraformaldehyde for 30 min at room temperature and stained with 0.1% crystal violet for 2 h at room temperature. Non-migratory cells located on the upper side of the membrane were gently removed using cotton wool and cells on the lower side of the membrane were semi-quantified. Representative images were captured by inverted fluorescence microscopy. Five random fields (x200 magnification) were selected and the average was calculated. The data are presented as the mean ± standard error from three independent experiments.

Xenograft tumor mouse model. Female BALB/c nude mice were purchased from Hunan SJA Laboratory Animal Co., Ltd. All animal experiments were conducted in strict accordance with guidelines approved by the Institutional Animal Care and Use Committee at Hunan Normal University (approval no. D2021059; Changsha, China). Female BALB/c nude mice (age, 6 weeks; weight, 18.0±2.0 g; n=6 mice/group) were subcutaneously injected with single-cell HepG2 lines into the right flanks of nude mice ($1x10^6$ cells in 100 μl PBS) on day 1. The mice were housed under controlled environmental conditions; the temperature was maintained at 22±2˚C and the relative humidity was kept at 50±10%. In addition, the mice had *ad libitum* access to food and water and were maintained under a 12-h light/dark cycle. Tumor volumes and mouse weight were determined every 2 days. Tumor size was measured using calipers, and tumor volume was calculated using the formula: 1/2 x [length x $(width)^2$]. After 15 days, all mice were deeply anesthetized with 1% pentobarbital sodium (40 mg/kg) to minimize any potential pain or distress during the procedure, followed by cervical dislocation to sacrifice the mice. Then tumors and major organs (liver and kidney) were removed for subsequent use in experiments. The humane experimental endpoints included tumor weight being >10% of animal body weight, tumor volume exceeding 2,000 mm^3, and weight loss of >20% animal body weight; no animals reached these criteria during the experiment.

Oil red O staining. Cells were seeded at a density of $4x10^4$ cells/well in 24-well culture plates. After 24 h, the cells were treated with AO (100 and 200 μM) for another 24 h at 37˚C. For the combined treatment, the cells were treated with AO (50 μM), PA (SK-Hep1: 10 μM, HepG2: 100 μM) or their combination at the indicated concentrations for 24 h at 37˚C. Then, cells in 24-cell dishes were washed with PBS and fixed with 4% paraformaldehyde for 20-30 min at room temperature, followed by another wash with PBS. Subsequently, the cells were incubated with Oil red O (0.5% in isopropanol; cat. no. 01391; Sigma-Aldrich; Merck KGaA) for 15 min at room temperature, were rinsed with 60% isopropanol for 30 sec and washed twice with distilled water. After washing, the cells were stained with hematoxylin (cat. no. BA40211; Baso Diagnostic Inc.) for 5 min at room temperature. After staining, the cells were washed with water to remove any unbound dye and were examined under a light microscope.

Histology. Tumor tissues from mice and human patients were fixed in 4% paraformaldehyde (Wuhan Servicebio Technology Co., Ltd.) for 24 h at room temperature, followed by embedding in paraffin and sectioning to a thickness of 7 μm. For histological analysis, the sections were rinsed three times with distilled water for 3 min. The sections were stained with hematoxylin for 3 min and eosin for 15-30 sec at room temperature (both from Wuhan Servicebio Technology Co., Ltd.) and evaluated for disease grading by a certified pathologist. For immunohistochemistry, the sections were deparaffinized and rehydrated using a sequence of xylene, 100, 95 and 75% ethanol. The sections were incubated with 3% H_2O_2 for

20 min at room temperature to quench endogenous peroxidase activity, washed with PBS, and boiled in Tris-EDTA retrieval solution for 5 min in a pressure cooker for antigen retrieval. After naturally cooling to room temperature, the sections were blocked with 10% goat serum (Beijing Solarbio Science & Technology Co., Ltd.) at room temperature for 20 min and incubated overnight at 4˚C with the anti-GPX4 (1:200; cat. no. DF6701; Affinity Biosciences) and anti-SCD1 (1:100; cat. no. A16429; Abclonal Biotech Co., Ltd.) primary antibodies. The sections were then washed with PBS and incubated with Reagent 2 (from the Goat Hypersensitivity Two-Step Detection Kit; cat. no. PV-9005; OriGene Technologies, Inc.) for 20 min at 37˚C. Subsequently, the sections were washed with PBS and incubated for 20 min at 37˚C with Reagent 3 (from the Goat Hypersensitivity Two-Step Detection Kit) following the manufacturer's instructions. The sections were washed again with PBS and stained using the DAB substrate kit (Cell Signaling Technology, Inc.), followed by counterstaining with Gill's hematoxylin (Beijing Solarbio Science & Technology Co., Ltd.). Finally, the sections were dehydrated and mounted using neutral resin (Beijing Solarbio Science & Technology Co., Ltd.).The slides were captured using an Olympus BX51 fluorescence microscope (Olympus Corporation).

Statistical analyses. All data are presented as the mean ± SD, or as the mean ± standard error of the mean for the Transwell assay. Each experiment was performed three times. Statistical analyses was performed using SPSS (version 16.0). Significance between two groups was evaluated using the unpaired Student's t-test, whereas the significance among multiple groups was determined using one-way analysis of variance followed by the Bonferroni significant difference test. Graphs were created using GraphPad Prism 6.0 (Dotmatics). $P<0.05$ was considered to indicate a statistically significant difference.

Results

AO inhibits liver cancer cell proliferation, colony formation and migration. To assess the anticancer activities of AO in liver cancer cells, its effect on the proliferation, colony formation and migration of liver cancer cells were investigated. As shown in Fig. 1A and B, AO treatment resulted in a concentration-dependent reduction in the viability and proliferation of liver cancer cells. The results of the colony formation assay demonstrated a dose-dependent inhibitory effect of AO (100-200 μM) (Fig. 1C). Notably, there was a significant difference in the sensitivity to AO between these two liver cancer cell lines, AO treatment exerted a more pronounced inhibitory effect on SK-Hep1 cells than on HepG2 cells (Fig. 1A). Subsequently, the present study assessed the effect of AO on cell migration. As shown in Fig. 1D, 200 μM AO exerted a significant inhibitory effect on the migration of these two cell lines compared with in the control group. These data suggested that AO effectively inhibited proliferation, colony formation and migration in liver cancer cells.

AO downregulates lipogenesis via SREBP1 and FASN. To assess the effect of AO treatment on lipid accumulation, Oil red O staining was employed to detect the alterations of lipids following various treatments. A marked reduction in the number of lipid bodies was observed in both SK-Hep1 and HepG2 cells after AO treatment (Fig. 2A). SREBP1 consists of both a precursor form (pSREBP1) and a mature form (mSREBP1). In the present study, AO significantly reduced the expression levels of both forms of SREBP1 and also inhibited the downstream expression of FASN (Fig. 2B). PA is a synthetic product of FASN, and the addition of PA can partially compensate for the function of FASN (45). The present study examined whether AO could reduce lipid levels in PA-treated liver cancer cells. First, the effect of PA on the viability of the liver cancer cell lines SK-Hep1 and HepG2 was examined (Fig. 2C), which indicated that there were significant differences in viability between cells treated with varying concentrations of PA and the control group. Furthermore, there were notable differences in the sensitivity of these two liver cancer cell lines to PA treatment; the IC_{50} value of PA in SK-Hep1 cells was markedly lower at 42.68 μM, compared with the substantially higher value of 348.71 μM in HepG2 cells. To prevent excessive lipid accumulation toxicity, 10 μM PA was selected for inducing lipid accumulation in SK-Hep1 cells and 100 μM PA was selected for HepG2 cells. PA induced lipid accumulation in both HepG2 and SK-Hep1 cells, whereas AO effectively reduced the number of lipid bodies induced by PA (Fig. 2D). Furthermore, the inhibitory effects of AO on the viability and colony formation of SK-Hep1 and HepG2 cells were partially reversed by PA (Fig. 2E and F). These results indicated that AO may inhibit the proliferation of liver cancer cells by suppressing fatty acid synthesis.

AO decreases SREBP1 expression by inactivating the AKT/mTOR signaling pathway. It has previously been shown that AKT and AMPK serve contrasting roles in fatty acid synthesis (46). The present study investigated the effect of AO on the protein expression levels of p-AKT, p-mTOR and p-AMPKα. AO treatment simultaneously reduced the protein expression levels of p-AKT, p-mTOR and p-AMPK. (Fig. 3A and B). Activation of AMPK can inhibit fatty acid synthesis and promote catabolism, thereby restoring cellular energy homeostasis; by contrast, inhibition of AMPK generally reduces its inhibitory effect on fatty acid synthesis (46). These findings suggested that AO may hinder SREBP1 expression by inactivating the AKT/mTOR pathway rather than activating AMPK. Furthermore, the viability of SK-Hep1 and HepG2 cells treated with a combination of an AKT inhibitor (MK2206) and AO was markedly reduced compared with that of cells treated with either MK2206 or AO alone (Fig. 3C and D). MK2206 also amplified the AO-induced downregulation of p-AKT (Fig. 3E).

AO induces ferroptosis by inactivating Nrf2/HO-1/GPX4 signaling. Ferroptosis is an iron-dependent form of cell death triggered by lipid peroxidation, which is suppressed by GPX4, a key enzyme in mammals capable of reducing esterified phospholipid hydroperoxides (21,35). To elucidate the relationship between AO and ferroptosis, the effect of AO on the expression of GPX4 was investigated. The results demonstrated that AO effectively suppressed the expression of GPX4 in both SK-Hep1 and HepG2 cells in a dose-dependent manner (Fig. 4A and B). Furthermore, the intracellular levels of LPO in these cells were assessed. After treatment with AO,

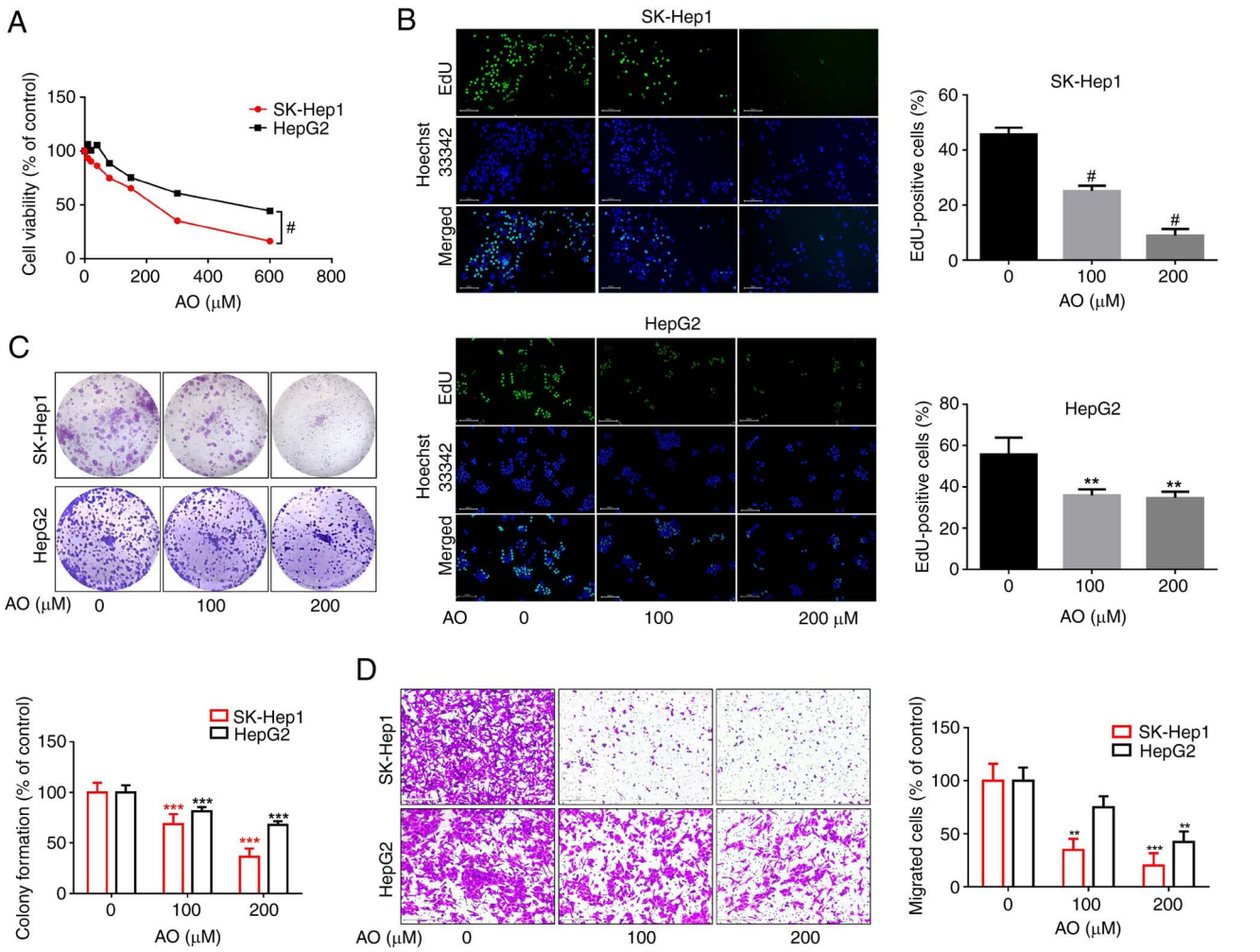

Figure 1. AO inhibits the viability, proliferation and migration of liver cancer cells. The effect of AO on liver cancer cell viability and proliferation was assessed by (A) Cell Counting Kit-8 assay and (B) EdU staining, respectively. #P<0.0001. Magnification, x200. (C) Effects of AO on the colony formation of SK-Hep1 and HepG2 cells. (D) Transwell assay was used to assess the migration of liver cancer cells after AO treatment. Magnification, x200. **P<0.01, ***P<0.001, #P<0.0001 vs. 0 μM. n=3. AO, aurantio-obtusin.

there was a significant increase in LPO levels (Fig. 4C and D). These results suggested that AO may have the potential to induce ferroptosis. Increasing evidence has highlighted the pivotal role of the Nrf2/HO-1/GPX4 axis in mediating ferroptosis (47). To determine the effects of AO on the Nrf2/HO-1 signaling pathway, western blot analysis was conducted. The results showed that AO significantly suppressed the expression of Nrf2 and HO-1 in SK-Hep1 and HepG2 cells (Fig. 4E-G). These findings suggested that AO may downregulate GPX4 expression and induce ferroptosis in liver cancer cells by inhibiting the Nrf2/HO-1 signaling pathway.

SCD1 expression levels are associated with ferroptosis sensitivity in liver cancer cells. The present study investigated the sensitivity of liver cancer cells to RSL3, a ferroptosis inducer, and observed notable variations in the responsiveness of SK-Hep1 and HepG2 cells to ferroptosis. As shown in Fig. 5A, treatment with 0.8 nM RSL3 led to a 90% inhibition of SK-Hep1 cell viability, but had no noticeable effect on HepG2 cells. SCD1, an enzyme responsible for converting saturated fatty acids into MUFAs, renders cancer cells sensitive to ferroptosis when genetically or pharmacologically inhibited. The present study assessed the baseline levels of SCD1 expression in SK-Hep1 and HepG2 cells, and detected significantly lower SCD1 and GPX4 expression in SK-Hep1 cells and relatively higher levels in HepG2 cells (Fig. 5B). Additionally, treatment with A939572, an inhibitor of SCD1 activity, enhanced the susceptibility of cancer cells to ferroptosis induction and lipid peroxidation compared with the control group (Fig. 5C-F). Subsequently, the preset study explored the potential mechanisms underlying ferroptosis sensitization by blocking SCD1. Transient silencing was performed using siRNAs to modulate SCD1 expression levels in liver cancer cells. Notably, SCD1 knockdown significantly reduced SCD1 protein expression but had no effect on GPX4 protein expression, suggesting that silencing SCD1 itself did not regulate GPX4 activity (Fig. 5G). Furthermore, silencing SCD1 or pharmacologically inhibiting SCD1 using A939572 amplified RSL3-reduced GPX4 protein levels (Fig. 5H and I). This finding suggested that inhibiting SCD1 may enhance the sensitivity of liver cancer cells to ferroptosis induction. In summary, these findings indicated that SCD1 may have a crucial role in determining the sensitivity of liver cancer cells to ferroptosis.

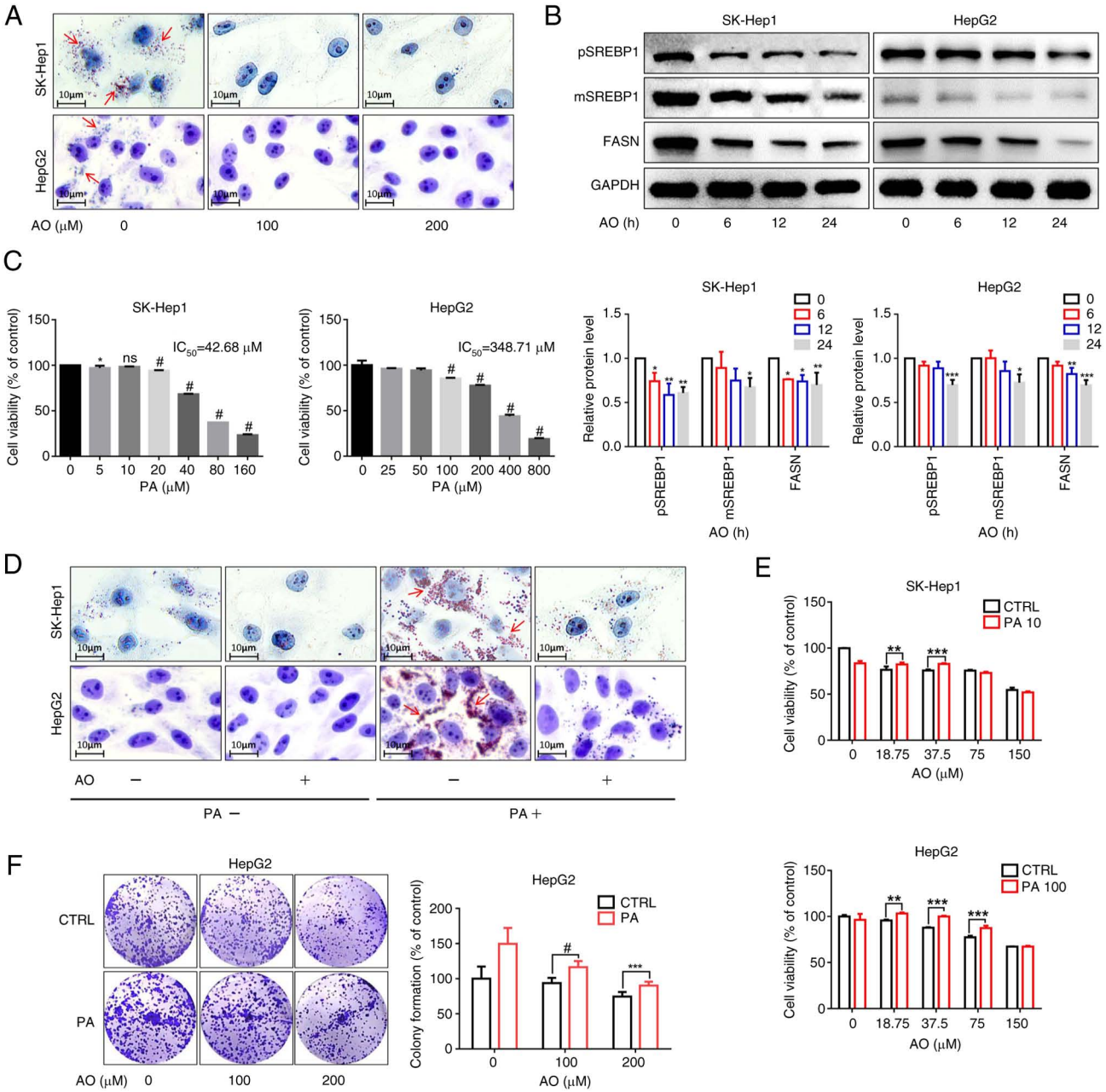

Figure 2. AO downregulates lipogenesis via the SREBP1 and FASN axis. (A) SK-Hep1 and HepG2 cells were exposed to AO for 24 h and then subjected to Oil red O assay for the detection of lipid droplets. Lipid droplets are indicated with red arrows. (B) SK-Hep1 and HepG2 cells were treated with 100 μM AO for 0, 6, 12 and 24 h, and western blot analysis was used to examine the expression of pSREBP1, mSREBP1 and FASN; GAPDH was included as a loading control. *P<0.05, **P<0.01, ***P<0.001 vs. 0 h. (C) CCK-8 assay evaluated the effects of PA on SK-Hep1 and HepG2 cell viability. *P<0.05, $^{\#}$P<0.0001 vs. 0 μM. (D) SK-Hep1 and HepG2 cells were treated with 10 and 100 μM PA, respectively, and 100 μM AO for 24 h. Lipid droplets were visualized using Oil red O staining. Lipid droplets are indicated with red arrows. (E) SK-Hep1 and HepG2 cells were treated with different concentrations of AO combined with PA for 48 h, and cell viability was measured using the CCK-8 assay. (F) HepG2 cells were treated with different concentrations of AO combined with PA (100 μM) for 7 days, and colony formation was measured. **P<0.01, ***P<0.001, $^{\#}$P<0.0001. n=3. AO, aurantio-obtusin; CCK-8, Cell Counting Kit-8; CTRL, control; FASN, fatty acid synthase; mSREBP1, mature SREBP1; ns, not significant; PA, palmitic acid; pSREBP1, precursor SREBP1; SREBP1, sterol regulatory element-binding protein 1.

AO sensitizes liver cancer cells to RSL3-induced ferroptosis by suppressing SCD1 expression. As aforementioned, inhibiting SCD1 increased the susceptibility of liver cancer cells to RSL3-induced ferroptosis. SCD1 is a downstream target of SREBP1; therefore, the present study investigated whether AO affects SCD1 expression in liver cancer cells using western blot analysis. As shown in Fig. 6A, treatment with 200 μM AO for 24 h significantly downregulated SCD1 expression in the liver cancer cells. Moreover, the combination of AO and RSL3 significantly reduced cell viability and proliferation (Fig. 6B and D) and colony formation (Fig. 6C) compared with RSL3 or AO alone. These effects were reversed by Fer-1, an effective and selective ferroptosis inhibitor that prevents membrane lipid damage via a reductive mechanism, thereby reversing the inhibitory effect on cell viability (Fig. 6B). Concurrently, LPO levels were markedly increased and GPX4 levels were markedly reduced when AO was combined with RSL3 compared with the RSL3 treatment group

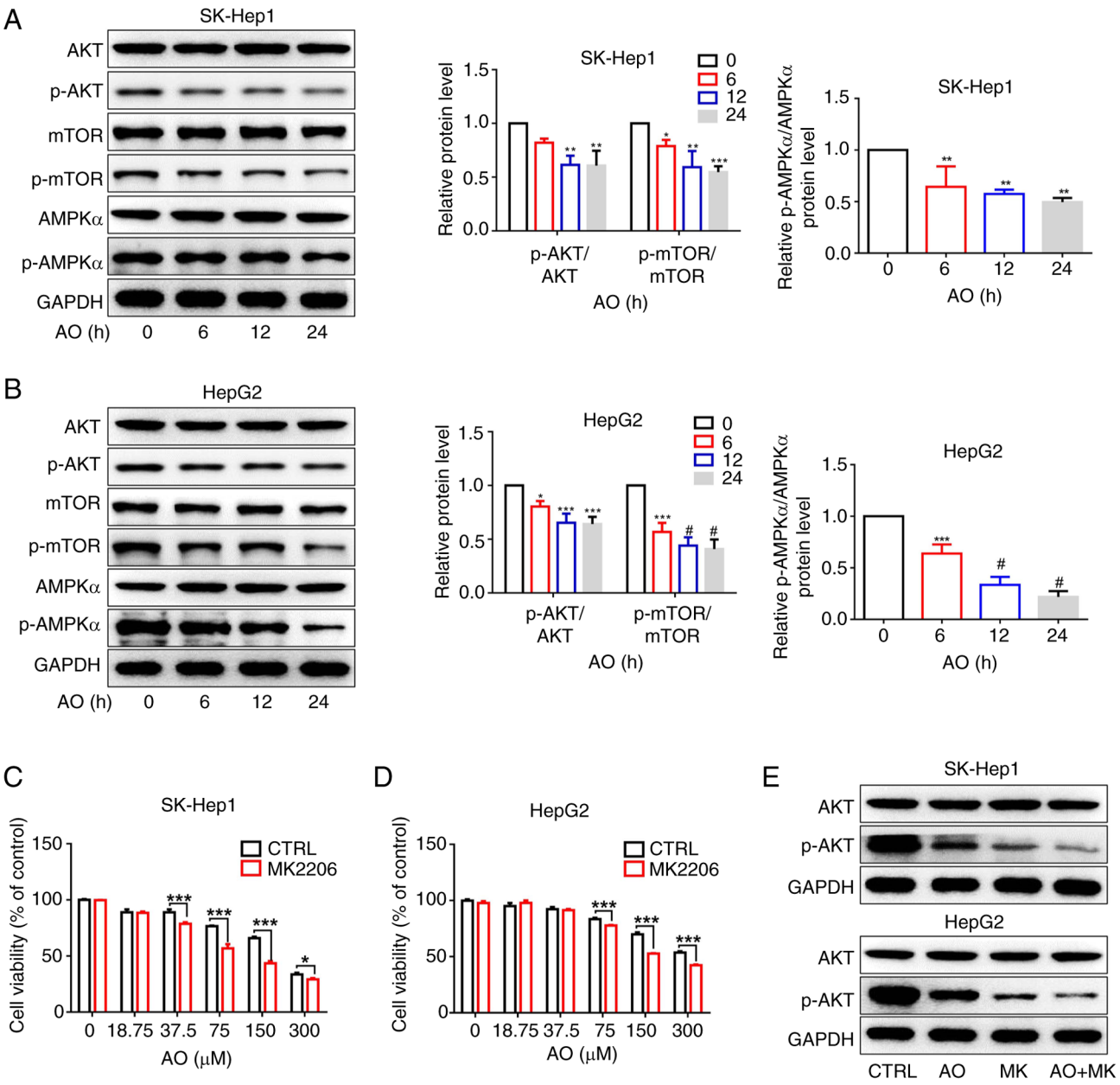

Figure 3. AO inhibits the expression of SREBP1 by inactivating the AKT/mTOR signaling pathway. (A) Protein expression levels of p-AKT, p-mTOR and p-AMPKα in SK-Hep1 and HepG2 cells were detected by western blotting after treatment with AO (100 μM) for different durations (0, 6, 12 and 24 h). *P<0.05, **P<0.01, ***P<0.001 vs. 0 h. (B) Protein expression levels of p-AKT, p-mTOR and p-AMPKα were semi-quantified. *P<0.05, ***P<0.001, $^{\#}$P<0.0001 vs. 0 h. (C) SK-Hep1 and (D) HepG2 cells were treated with different concentrations of AO combined with MK2206 (1 μM) for 48 h, and cell viability was measured using the cell counting Kit-8 assay. (E) Protein expression levels of p-AKT were detected by western blotting in SK-Hep1 and HepG2 cells treated with AO (50 μM), MK2206 (1 μM) or the combination for 24 h. *P<0.05, ***P<0.001. n=3. AMPKα, AMP-activated protein kinase α; AO, aurantio-obtusin; mTOR, mammalian target of rapamycin; p-, phosphorylated.

(Fig. 6E and F). In summary, these results suggested that AO enhanced RSL3-induced ferroptosis in liver cancer cells by inhibiting SCD1 expression.

Antitumor efficacy of AO and RSL3 combined therapy in a human liver cancer xenograft model. To further explore the potential anticancer therapeutic benefits of simultaneous AO and RSL3 treatment *in vivo*, experiments were conducted using a human liver cancer xenograft model in nude mice. Mice subcutaneously injected with HepG2 cells were treated with AO or RSL3, alone or in combination, for 15 days. Tumor growth was significantly slower in the combination treatment group than in the groups treated with AO or RSL3 alone (Fig. 7A and B). Furthermore, the tumor weight was markedly lower in the combination treatment group than in the other groups (Fig. 7C). Throughout the course of the animal study, total body weight was monitored as an indicator of treatment-related toxicity. No significant weight loss was observed in any of the treatment groups (Fig. 7D), indicating that the treatments were well-tolerated. Additionally, a decrease in GPX4 expression was observed in the tumors from the combination treatment group compared with the RSL3 group (Fig. 7E). Similarly, no hepatic or renal toxicity was observed after AO treatment (Fig. 7F). In summary, these

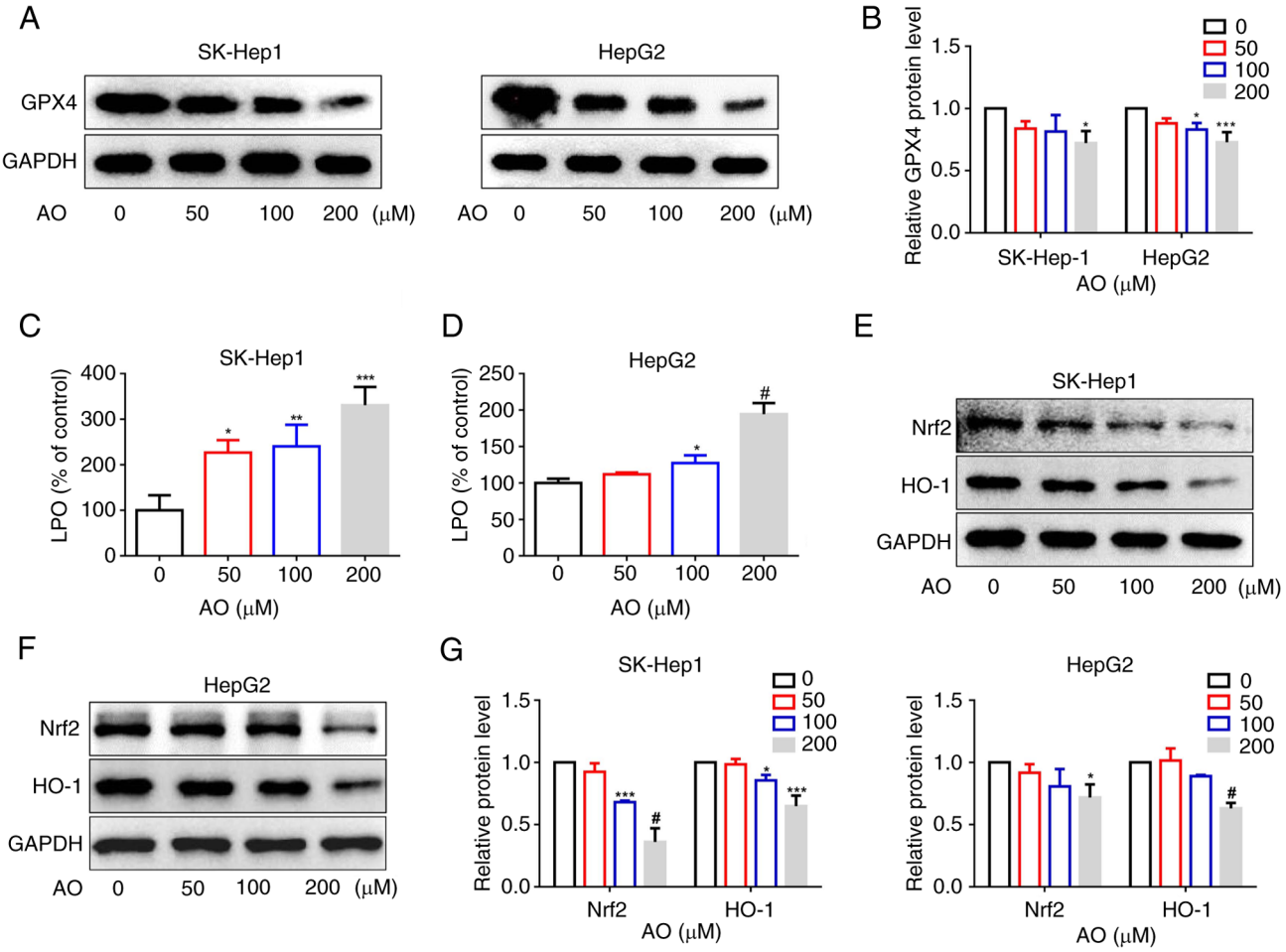

Figure 4. AO induces ferroptosis by inactivating Nrf2/HO-1/GPX4 signaling. (A and B) SK-Hep1 and HepG2 cells were treated with AO (0, 50, 100 or 200 μM) for 24 h, and the protein expression levels of GPX4 were measured by western blotting. (C) SK-Hep1 and (D) HepG2 cells were treated with AO for 24 h and lipid peroxidation levels were detected. (E-G) SK-Hep1 and HepG2 cells were treated with AO (0, 50, 100 or 200 μM) for 24 h, and the protein expression levels of Nrf2 and HO-1 were measured by western blotting. *P<0.05, **P<0.01, ***P<0.001, $^{\#}$P<0.0001 vs. 0 μM. n=3. AO, aurantio-obtusin; GPX4, glutathione peroxidase 4; HO-1, heme oxygenase 1; LPO, lipid peroxide; Nrf2, nuclear factor erythroid 2-related factor 2.

findings highlight the therapeutic potential of combining AO with a ferroptosis inducer in liver cancer treatment.

SCD1/GPX4 is differentially expressed in specimens from patients with liver cancer. To investigate the relationship between SCD1 and liver cancer progression, SCD1 expression w/as assessed in specimens from patients with liver cancer. Immunohistochemistry revealed a marked increase in SCD1 protein levels in liver cancer tissues compared with those in normal liver tissues (Fig. 8A). Furthermore, liver cancer samples from TCGA database, which included 371 primary liver tumor samples and 50 normal liver tissue samples, were analyzed. The results consistently demonstrated that SCD1 expression in primary liver tumors was significantly elevated compared with that in normal liver tissues (Fig. 8B). Notably, the bioinformatics analysis utilizing data from TCGA database also revealed a weak positive correlation between the expression levels of SCD1 and GPX4 in liver cancer tissues (Fig. 8C). Similarly, the immunohistochemistry analyses confirmed a substantial increase in GPX4 protein levels in liver cancer tissues compared with in normal liver tissues, consistent with the findings from TCGA database (Fig. 8D and E). These findings collectively suggested that both SCD1 and GPX4 were significantly upregulated in liver cancer tissues compared with in normal liver tissues, and have the potential to serve as valuable biomarkers for personalized treatment in patients with liver cancer.

Discussion

The present study conducted *in vivo* and *in vitro* experiments to investigate the inhibitory effects of AO on liver cancer cells. Lipid metabolism is frequently disrupted in cancer and some reports have suggested that abnormal lipid metabolism may serve an essential role in liver carcinogenesis (6,12,48). Altered *de novo* lipogenesis (DNL) is a pivotal deregulated metabolic event in cancer. SREBP1 controls the transcription of major enzymes involved in DNL, including ACLY, ACACA, FASN and SCD1. Previous studies have reported an increase in DNL in liver cancer samples (9,10,49,50). Multiple mechanisms, such as activation of the AKT/mTOR pathway, can lead to increased SREBP1 induction and enhanced expression of ACLY, ACACA, FASN and SCD1. In liver cancer, SCD1 has been reported to be upregulated and to be associated with shorter disease-free survival (32,51). This finding is consistent with the results of the present analysis using TCGA database.

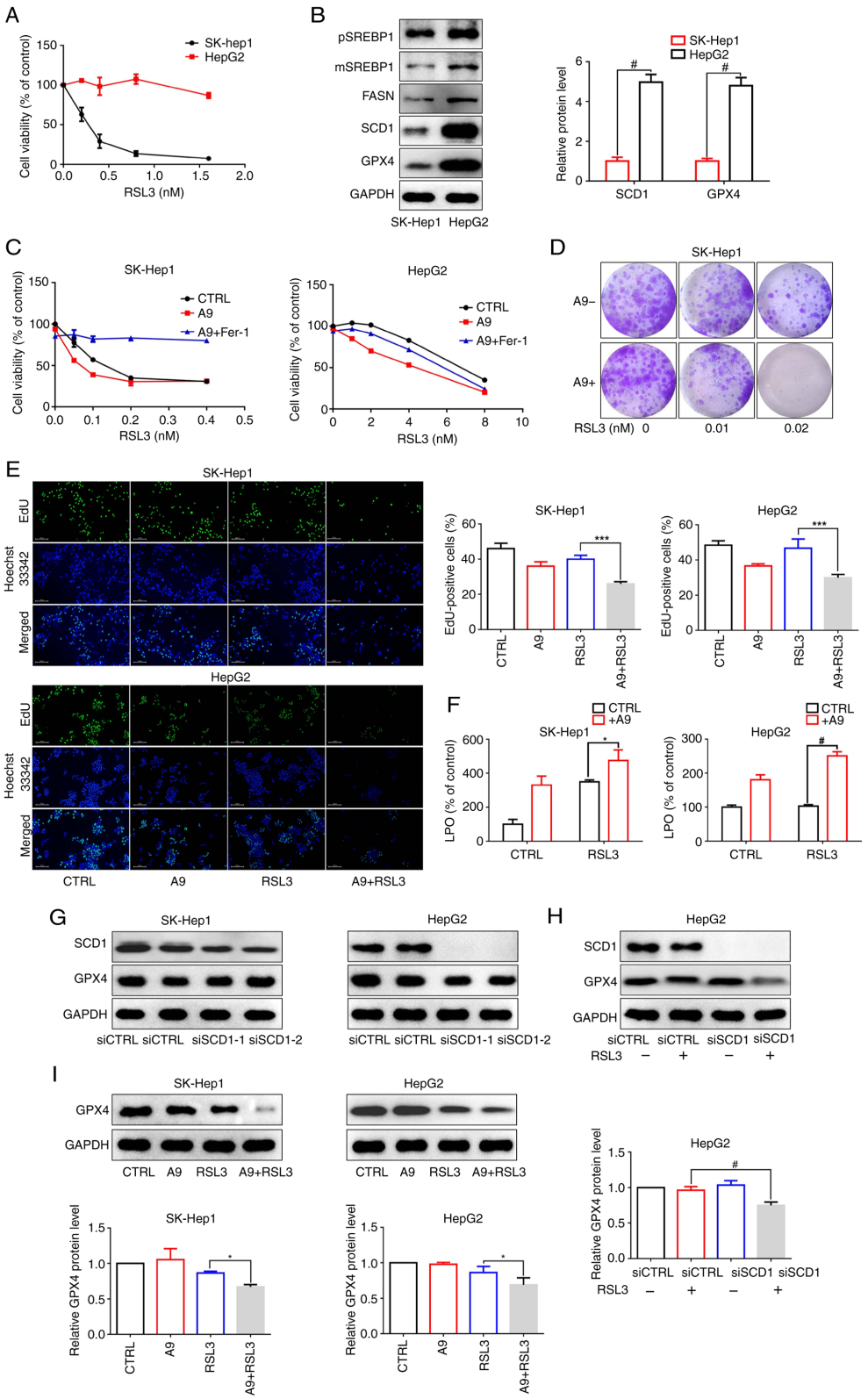

Figure 5. Relationship between SCD1 expression and the sensitivity of liver cancer cells to RSL3. (A) Cell Counting Kit-8 assay was used to evaluate the effects of RSL3 on SK-Hep1 and HepG2 cell viability. (B) Western blot analysis was performed to determine the basal levels of pSREBP1, mSREBP1, FASN, SCD1 and GPX4 protein expression in SK-Hep1 and HepG2 cells. (C) Cell viability was measured in SK-Hep1 and HepG2 cells treated with different concentration of RSL3, or a combination of A939572 (8 μM) and Fer-1 (5 nM) for 48. (D) SK-Hep1 cells were treated with different concentration of RSL3 combined with A939572 (8 μM) for 7 days, and colony formation was measured. (E and F) SK-Hep1 and HepG2 cells were treated with A939572 (8 μM), RSL3 (SK-Hep1: 0.01 nM, HepG2: 1 nM) or the combination for 24 h. (E) Cell proliferation was assessed by EdU staining (magnification, x200) and (F) lipid peroxidation levels were detected using the LPO Content Assay Kit. (G) Expression levels of GPX4 were measured by western blotting after transfection with siSCD1. (H) HepG2 cells were transfected with siCTRL or siSCD1 and then treated with RSL3 for 24 h, followed by western blot analysis of SCD1 expression. (I) Protein expression levels of GPX4 were detected in SK-Hep1 and HepG2 cells treated with A939572 (8 μM), RSL3 (SK-Hep1: 0.01 nM, HepG2: 1 nM), or their combination for 24 h. *P<0.05, ***P<0.001, $^{\#}$P<0.0001. n=3. CTRL, control; FASN, fatty acid synthase; Fer-1, ferrostatin-1; GPX4, glutathione peroxidase 4; LPO, lipid peroxide; mSREBP1, mature SREBP1; pSREBP1, precursor SREBP1; SCD1, stearoyl-CoA desaturase 1; si, small interfering; SREBP1, sterol regulatory element-binding protein 1.

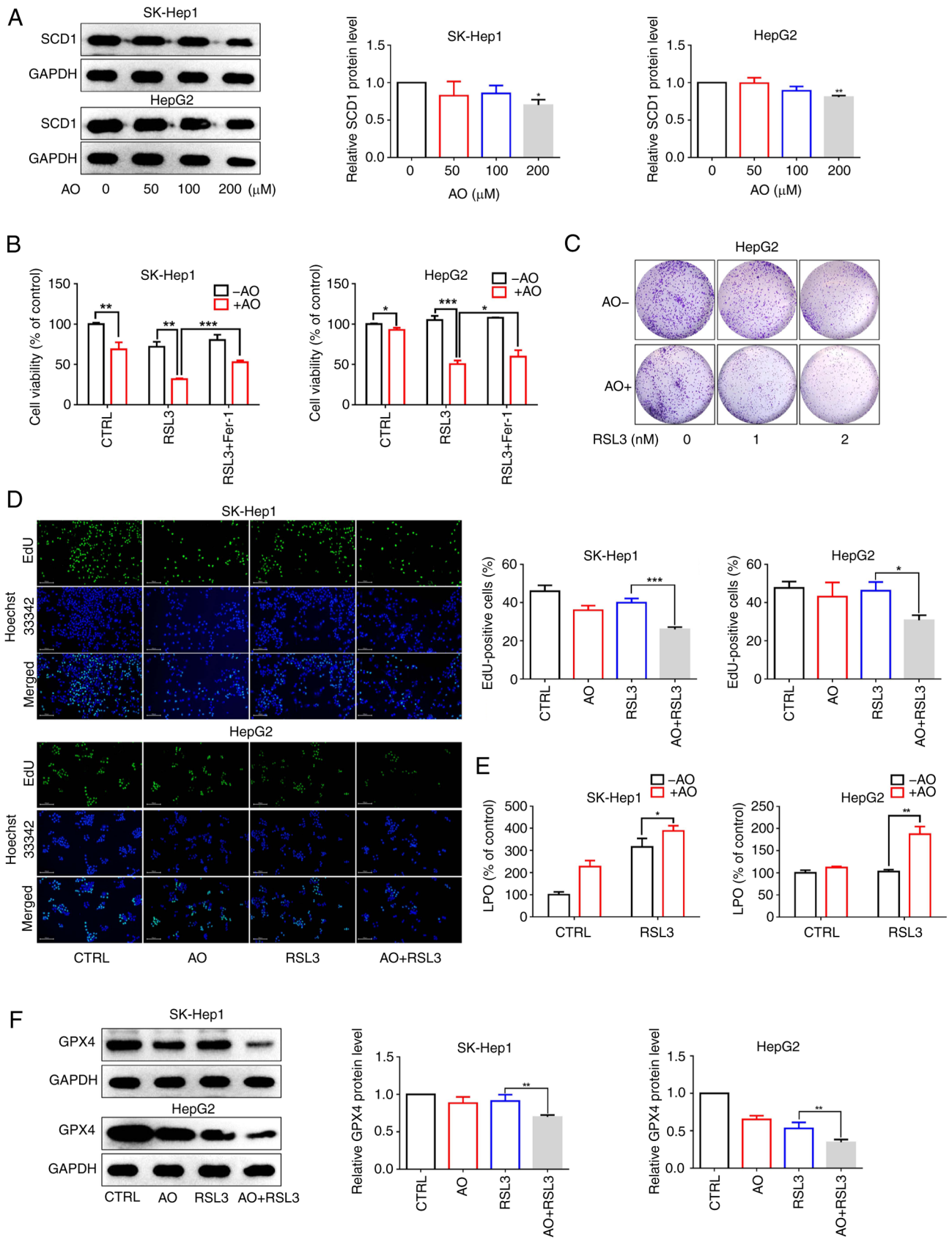

Figure 6. AO sensitizes liver cancer cells to ferroptosis by suppressing SCD1 expression. (A) Expression levels of SCD1 protein in cells treated with AO for 24 h. *P<0.05, **P<0.01 vs. 0 μM. (B) Cell viability was measured in SK-Hep1 and HepG2 cells treated with AO (50 μM), RSL3 (SK-Hep1: 0.01 nM, HepG2: 1 nM), or the combination in the presence or absence of Fer-1 (5 nM) for 48 h. (C) HepG2 cells were treated with different concentration of RSL3 combined with AO (50 μM) for 7 days, and colony formation was measured. (D and E) SK-Hep1 and HepG2 cells treated with AO (50 μM), RSL3 (SK-Hep1: 0.01 nM, HepG2: 1 nM) or the combination for 24 h. (D) Cell proliferation was assessed by EdU staining (magnification, x200) and (E) lipid peroxidation levels were detected using the Lipid Peroxide Content Assay Kit. (F) Protein expression levels of GPX4 were detected in SK-Hep1 and HepG2 cells treated with AO (50 μM), RSL3 (SK-Hep1: 0.01 nM, HepG2: 1 nM), or their combination for 24 h. *P<0.05, **P<0.01, ***P<0.001. n=3. AO, aurantio-obtusin; CTRL control; Fer-1, ferrostatin-1; GPX4, glutathione peroxidase 4; LPO, lipid peroxide; SCD1, stearoyl-CoA desaturase 1.

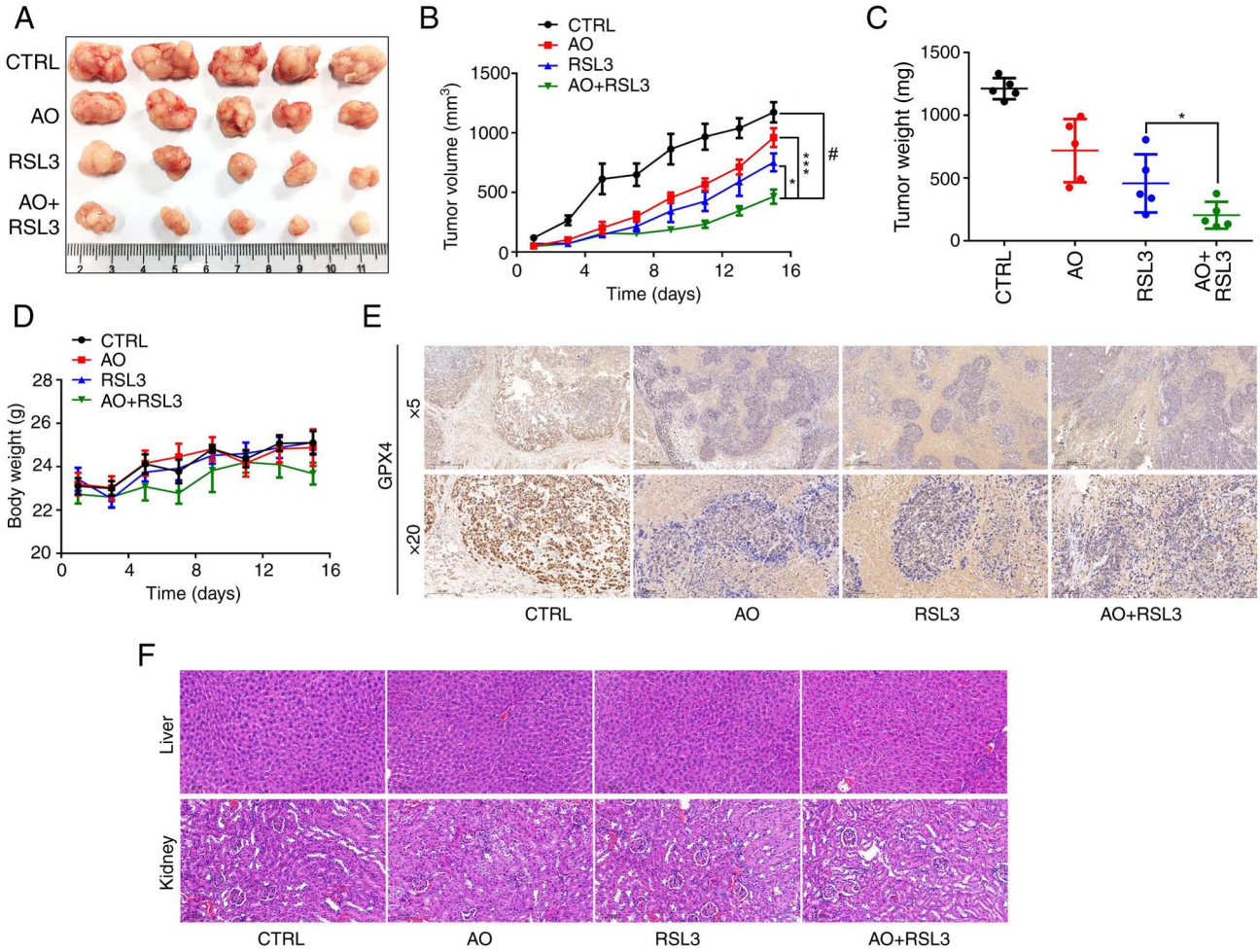

Figure 7. The antitumor efficacy of combined AO and RSL3 therapy was evaluated in a human liver cancer cell xenograft model. (A) Images, (B) volume and (C) weight of xenograft tumors from various mouse groups were recorded after 15 days of treatment. (D) Body weight of mice was measured every 2 days after the xenograft mouse model was established. (E) Tumor tissues were subjected to immunostaining for GPX4. (F) No hepatic or renal toxicity was observed after AO treatment. Magnification, x200. *P<0.05, ***P<0.001, $^{\#}$P<0.0001. n=5. AO, aurantio-obtusin; CTRL, control; GPX4, glutathione peroxidase 4.

In addition, in a combined proteomic and lipidomic profiling study, upregulated hepatic SCD1 was identified as a reliable marker for liver cancer diagnosis and progression (52). A previous study demonstrated contrasting roles for AKT and AMPK in fatty acid synthesis (46). Mechanistically, SCD1 expression is induced by the AKT/mTOR pathway, whereas AMPK suppresses its expression (53-56). The present study confirmed that AO can inhibit the expression of SCD1 by suppressing the AKT/mTOR/SREBP1 pathway, rather than the AMPK pathway.

Ferroptosis is a form of programmed cell death triggered by metabolically regulated lipid peroxidation. Notably, it can enhance the effectiveness of both targeted therapy and chemotherapy in the treatment of cancer (57). The present study observed that lower SCD1 expression led to increased susceptibility to ferroptosis in SK-Hep1 and HepG2 cancer cell lines. SCD1-catalyzed MUFAs effectively suppress ferroptosis by substituting polyunsaturated fatty acids in the lipid membrane, thereby reducing the accumulation of lipid ROS (58). SCD1 has been extensively studied for a number of years in the context of metabolic diseases, such as diabetes and obesity (59,60). However, to the best of our knowledge, the exact role of SCD1 in the development of cancer remains unclear. It has been indicated that SCD1 has a crucial role in the regulation of liver tumor-initiating cells and sorafenib resistance by modulating endoplasmic reticulum stress-mediated differentiation (51). In the present study, it was observed that the combination of A939572 and RSL3 led to a significant inhibition of proliferation and a marked decrease in colony formation in SK-Hep1 and HepG2 cancer cells. This suggests that the combination of SCD1 inhibitors with ferroptosis inducers may enhance the anti-liver cancer effects of ferroptosis inducers.

In mammalian cells, the GSH-GPX4 axis serves a pivotal role in scavenging LPO, thereby inhibiting ferroptosis (61-63). Inhibition of the Nrf2/HO-1 pathway could suppress the expression of GPX4 (47). Recent studies have demonstrated that the downregulation of GPX4 expression induces the accumulation of LPO, promoting ferroptosis and resulting in increased sensitivity of resistant liver cancer cells to sorafenib (24,64). Consequently, triggering ferroptosis is recognized as a valuable approach to resensitize liver cancer cells to therapies. Recent research has revealed that GPX4 is a downstream target of SCD1/FADS2 (65). SCD1/FADS2 act as a positive regulator of GPX4 and modulates the GSH/GSSG ratio to prevent an excessive accumulation of ROS, thereby mediating oxidative stress and ferroptosis in ascites-derived ovarian cancer cells (65).

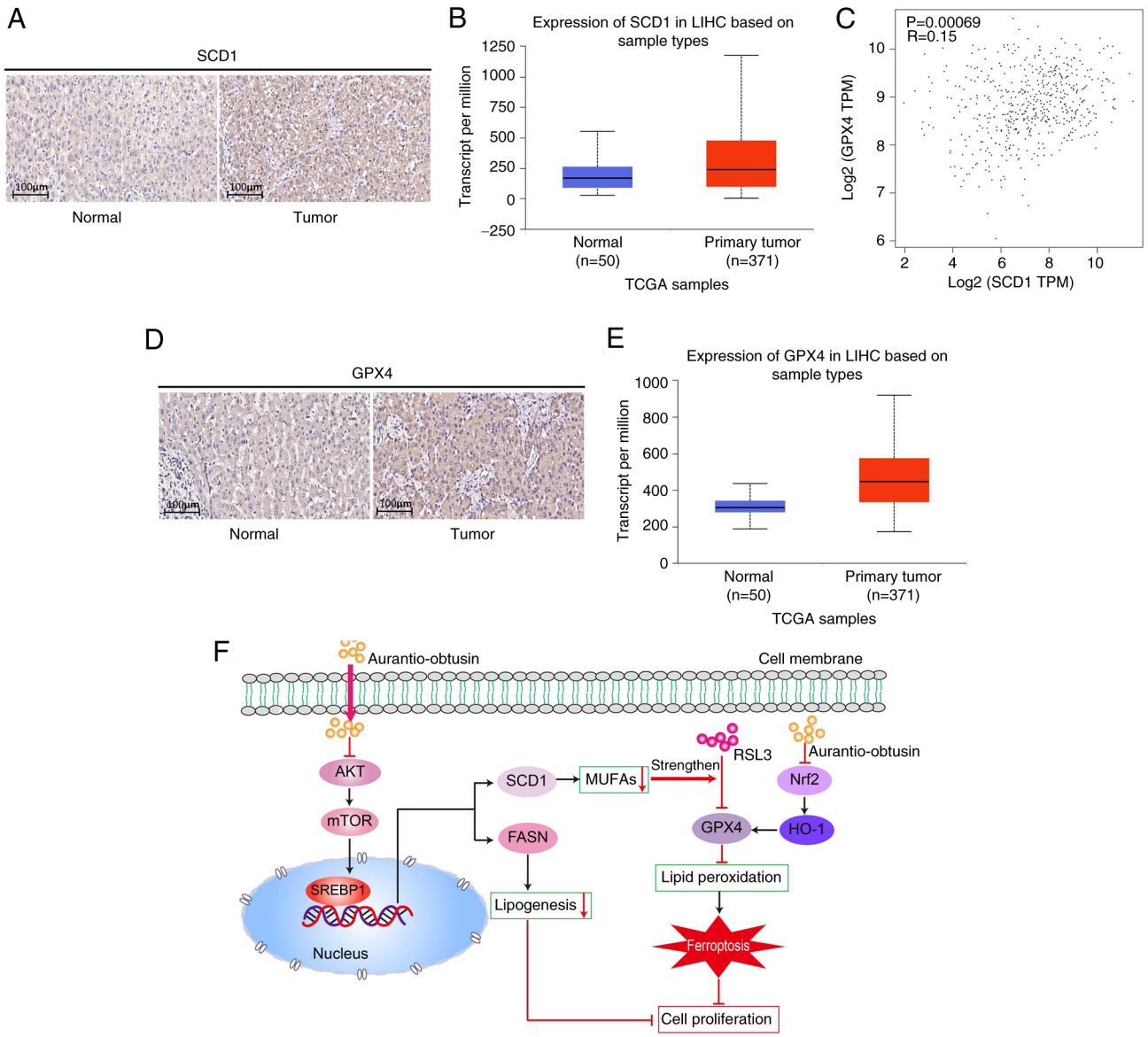

Figure 8. SCD1 and GPX4 are differentially expressed in specimens from patients with liver cancer. (A) Representative images showing protein expression of SCD1 in human liver cancer tissues and normal liver tissues. (B) The relative mRNA expression levels of SCD1 in liver cancer tissues were obtained from TCGA database. (C) Correlation between SCD1 and GPX4 based on TCGA data. (D) Representative protein expression of GPX4 in human liver cancer tissues and normal liver tissues. (E) The relative mRNA expression levels of GPX4 in liver cancer tissues were obtained from TCGA database. (F) A diagram showing the mechanism by which aurantio-obtusin induces ferroptosis by suppressing the Nrf2/HO-1 pathway and enhances RSL3-induced ferroptosis by inhibiting the AKT/mTOR/SREBP-1/SCD1 axis. FASN, fatty acid synthase; GPX4, glutathione peroxidase 4; HO-1, heme oxygenase 1; LIHC, liver hepatocellular carcinoma; mTOR, mammalian target of rapamycin; MUFAs, monounsaturated fatty acids; Nrf2, nuclear factor erythroid 2-related factor 2; SCD1, stearoyl-CoA desaturase 1; SREBP1, sterol regulatory element-binding protein 1.

AO, an anthraquinone monomer compound derived from cassia seeds, has been the subject of modern pharmacological studies (38,40,41). These studies have demonstrated the efficacy of AO in reducing blood lipid levels, mitigating NAFLD and exhibiting anti-influenza properties (37,38,40). Despite its diverse effects, the potential therapeutic advantages of AO in cancer treatment remain unclear. In the present study, it was shown that AO treatment at micromolar concentrations could effectively reduce cell proliferation and migration, while impeding *de novo* fatty acid synthesis in liver cancer cells.

The present study investigated the anti-liver cancer effects of AO in cellular and animal models. The findings demonstrated that AO could effectively inhibit the growth of human liver cancer cells in a xenograft tumor mouse model. Furthermore, the synergistic application of AO with the ferroptosis inducer RSL3 exhibited superior inhibitory effects compared with their individual use. Mechanistic insights from cell experiments revealed that AO attenuated proliferation and migration of liver cancer cells, and this action was mediated through inhibition of the AKT/mTOR/SREBP1 signaling pathway, downregulation of SCD1, suppression of lipid synthesis and concurrent inhibition of GPX4 by Nrf2/HO-1 pathway, ultimately leading to the induction of ferroptosis and anti-liver cancer effects (Fig. 8F). Additionally, the enhanced inhibition of SCD1 by AO further augmented the induction of ferroptosis by the ferroptosis inducer RSL3 (Fig. 8F). These findings highlight the potential therapeutic efficacy of AO in combating liver cancer and underscore the importance of targeting ferroptosis as a promising strategy

for cancer therapy. Although the present findings indicated that AO may induce ferroptosis in liver cancer cells by inhibiting the Nrf2/HO-1/GPX4 signaling pathway, the investigation of this mechanism remains insufficient. To confirm that this is the sole pathway through which AO regulates ferroptosis, further studies utilizing a GPX4-knockdown model are necessary.

Acknowledgements

The authors would like to thank Ms. Xin Ying (School of Medicine of Hunan Normal University, Changsha, China) for their assistance in editing the diagram.

Funding

This work was supported by the Hunan Provincial Natural Science Foundation (grant nos. 2023JJ30348, 2021JJ8028 and 2022JJ80073), the Hunan Health Commission High-level Talent Project (grant no. 20230609-1014), the Hunan Administration of Traditional Chinese Medicine (grant no. 201922) and the Scientific Research Project of the Changsha Science and Technology Department (grant no. kq2208125).

Availability of data and materials

The data generated in the present study may be requested from the corresponding author.

Authors' contributions

LJT and HWD designed the study, confirmed the authenticity of all the raw data and revised the manuscript. XJT provided ethical oversight for the animal experiments and performed the experiments. WL and JD analyzed the data and wrote the manuscript. WL, JD, XDC, YP and XCQ performed the experiments. All authors read and approved the final version of the manuscript.

Ethics approval and consent to participate

This study adhered to the guidelines for animal and human research ethics. Animal experiments were conducted following protocols approved by the Institutional Animal Care and Use Committee at Hunan Normal University (approval no. D2021059). Human study protocols were approved by the Ethics Committee of Hunan Provincial People's Hospital, Changsha, China [approval no. (2023)-178]. The patients provided informed consent for their tissues to be used in future research at the time of initial collection. Consequently, the requirement for informed consent was waived by the same committee due to the retrospective nature of the study and the use of anonymized data.

Patient consent for publication

Not applicable.

Competing interests

The authors declare that they have no competing interests.

References

1. Bray F, Ferlay J, Soerjomataram I, Siegel RL, Torre LA and Jemal A: Global cancer statistics 2018: GLOBOCAN estimates of incidence and mortality worldwide for 36 cancers in 185 countries. CA Cancer J Clin 68: 394-424, 2018.
2. Chen D, Wang J, Li Y, Xu C, Fanzheng M, Zhang P and Liu L: LncRNA NEAT1 suppresses cellular senescence in hepatocellular carcinoma via KIF11-dependent repression of CDKN2A. Clin Transl Med 13: e1418, 2023.
3. Wang L, Liu BX and Long HY: Ablative strategies for recurrent hepatocellular carcinoma. World J Hepatol 15: 515-524, 2023.
4. Aravinthan AD, Bruni SG, Doyle AC, Thein HH, Goldaracena N, Issachar A, Lilly LB, Selzner N, Bhat M, Sreeharsha B, *et al*: Liver transplantation is a preferable alternative to palliative therapy for selected patients with advanced hepatocellular carcinoma. Ann Surg Oncol 24: 1843-1851, 2017.
5. Shukla A, Patkar S, Sundaram S, Shah SR, Ingle M, Gupta A, Gopan A, Kamat M, Mohanka R, Singh S, *et al*: Clinical profile, patterns of care & adherence to guidelines in patients with hepatocellular carcinoma: Prospective multi-center study. J Clin Exp Hepatol 12: 1463-1473, 2022.
6. Nakagawa H, Hayata Y, Kawamura S, Yamada T, Fujiwara N and Koike K: Lipid metabolic reprogramming in hepatocellular carcinoma. Cancers (Basel) 10: 447, 2018.
7. Balsano C, Porcu C, Sideri S and Tavolaro S: Fat and hepatocellular carcinoma. Hepatoma Res 4: 38, 2018.
8. Scheinberg T, Mak B, Butler L, Selth L and Horvath LG: Targeting lipid metabolism in metastatic prostate cancer. Ther Adv Med Oncol 15: 17588359231152839, 2023.
9. Fhu CW and Ali A: Fatty acid synthase: An emerging target in cancer. Molecules 25: 3935, 2020.
10. Jones SF and Infante JR: Molecular pathways: Fatty acid synthase. Clin Cancer Res 21: 5434-5438, 2015.
11. Koundouros N and Poulogiannis G: Reprogramming of fatty acid metabolism in cancer. Br J Cancer 122: 4-22, 2020.
12. Qin XY, Su T, Yu W and Kojima S: Lipid desaturation-associated endoplasmic reticulum stress regulates MYCN gene expression in hepatocellular carcinoma cells. Cell Death Dis 11: 66, 2020.
13. Wang H, Zhou Y, Xu H, Wang X, Zhang Y, Shang R, O'Farrell M, Roessler S, Sticht C, Stahl A, *et al*: Therapeutic efficacy of FASN inhibition in preclinical models of HCC. Hepatology 76: 951-966, 2022.
14. Wang X, Liu Y, Han A, Tang C, Xu R, Feng L, Yang Y, Chen L and Lin Z: The NQO1/p53/SREBP1 axis promotes hepatocellular carcinoma progression and metastasis by regulating Snail stability. Oncogene 41: 5107-5120, 2022.
15. Li C, Yang W, Zhang J, Zheng X, Yao Y, Tu K and Liu Q: SREBP-1 has a prognostic role and contributes to invasion and metastasis in human hepatocellular carcinoma. Int J Mol Sci 15: 7124-7138, 2014.
16. Shimano H and Sato R: SREBP-regulated lipid metabolism: Convergent physiology-divergent pathophysiology. Nat Rev Endocrinol 13: 710-730, 2017.
17. Peterson TR, Sengupta SS, Harris TE, Carmack AE, Kang SA, Balderas E, Guertin DA, Madden KL, Carpenter AE, Finck BN and Sabatini DM: mTOR complex 1 regulates lipin 1 localization to control the SREBP pathway. Cell 146: 408-420, 2011.
18. Bakan I and Laplante M: Connecting mTORC1 signaling to SREBP-1 activation. Curr Opin Lipidol 23: 226-234, 2012.
19. Tao T, Su Q, Xu S, Deng J, Zhou S, Zhuang Y, Huang Y, He C, He S, Peng M, *et al*: Down-regulation of PKM2 decreases FASN expression in bladder cancer cells through AKT/mTOR/SREBP-1c axis. J Cell Physiol 234: 3088-3104, 2019.
20. Li Y, Yang W, Zheng Y, Dai W, Ji J, Wu L, Cheng Z, Zhang J, Li J, Xu X, *et al*: Targeting fatty acid synthase modulates sensitivity of hepatocellular carcinoma to sorafenib via ferroptosis. J Exp Clin Cancer Res 42: 6, 2023.
21. Ursini F and Maiorino M: Lipid peroxidation and ferroptosis: The role of GSH and GPx4. Free Radic Biol Med 152: 175-185, 2020.
22. Wang Z, Zhou C, Zhang Y, Tian X, Wang H, Wu J and Jiang S: From synergy to resistance: Navigating the complex relationship between sorafenib and ferroptosis in hepatocellular carcinoma. Biomed Pharmacother 170: 116074, 2024.
23. Dahiya M and Dureja H: Sorafenib for hepatocellular carcinoma: Potential molecular targets and resistance mechanisms. J Chemother 34: 286-301, 2022.
24. Wang C, Zheng C, Wang H, Shui S, Jin H, Liu G, Xu F, Liu Z, Zhang L, Sun D and Xu P: Dual degradation mechanism of GPX4 degrader in induction of ferroptosis exerting anti-resistant tumor effect. Eur J Med Chem 247: 115072, 2023.

25. Tang W, Chen Z, Zhang W, Cheng Y, Zhang B, Wu F, Wang Q, Wang S, Rong D, Reiter FP, *et al*: The mechanisms of sorafenib resistance in hepatocellular carcinoma: Theoretical basis and therapeutic aspects. Signal Transduct Target Ther 5: 87, 2020.
26. Gao Z, Wang D, Yang J, Li M, Ling C, Lv D, Cao Y, Chen Z, Shi C, Shen H and Tang Y: Iron deficiency in hepatocellular carcinoma cells induced sorafenib resistance by upregulating HIF-1α to inhibit apoptosis. Biomed Pharmacother 163: 114750, 2023.
27. Menendez JA and Lupu R: Fatty acid synthase and the lipogenic phenotype in cancer pathogenesis. Nat Rev Cancer 7: 763-777, 2007.
28. Raeisi M, Hassanbeigi L, Khalili F, Kharrati-Shishavan H, Yousefi M and Mehdizadeh A: Stearoyl-CoA desaturase 1 as a therapeutic target for cancer: A focus on hepatocellular carcinoma. Mol Biol Rep 49: 8871-8882, 2022.
29. Guo Z, Huo X, Li X, Jiang C and Xue L: Advances in regulation and function of stearoyl-CoA desaturase 1 in cancer, from bench to bed. Sci China Life Sci 66: 2773-2785, 2023.
30. Sen U, Coleman C and Sen T: Stearoyl coenzyme A desaturase-1: Multitasker in cancer, metabolism, and ferroptosis. Trends Cancer 9: 480-489, 2023.
31. Liu HH, Xu Y, Li CJ, Hsu SJ, Lin XH, Zhang R, Chen J, Chen J, Gao DM, Cui JF, *et al*: An SCD1-dependent mechanoresponsive pathway promotes HCC invasion and metastasis through lipid metabolic reprogramming. Mol Ther 30: 2554-2567, 2022.
32. Bansal S, Berk M, Alkhouri N, Partrick DA, Fung JJ and Feldstein A: Stearoyl-CoA desaturase plays an important role in proliferation and chemoresistance in human hepatocellular carcinoma. J Surg Res 186: 29-38, 2014.
33. Wang C, Shi M, Ji J, Cai Q, Zhao Q, Jiang J, Liu J, Zhang H, Zhu Z and Zhang J: Stearoyl-CoA desaturase 1 (SCD1) facilitates the growth and anti-ferroptosis of gastric cancer cells and predicts poor prognosis of gastric cancer. Aging (Albany NY) 12: 15374-15391, 2020.
34. Tesfay L, Paul BT, Konstorum A, Deng Z, Cox AO, Lee J, Furdui CM, Hegde P, Torti FM and Torti SV: Stearoyl-CoA desaturase 1 protects ovarian cancer cells from ferroptotic cell death. Cancer Res 79: 5355-5366, 2019.
35. Yang WS and Stockwell BR: Ferroptosis: Death by lipid peroxidation. Trends Cell Biol 26: 165-176, 2016.
36. Chen H, Qi Q, Wu N, Wang Y, Feng Q, Jin R and Jiang L: Aspirin promotes RSL3-induced ferroptosis by suppressing mTOR/SREBP-1/SCD1-mediated lipogenesis in PIK3CA-mutant colorectal cancer. Redox Biol 55: 102426, 2022.
37. Kim M, Lim SJ, Lee HJ and Nho CW: *Cassia tora* seed extract and its active compound aurantio-obtusin inhibit allergic responses in IgE-mediated mast cells and anaphylactic models. J Agric Food Chem 63: 9037-9046, 2015.
38. Kwon KS, Lee JH, So KS, Park BK, Lim H, Choi JS and Kim HP: Aurantio-obtusin, an anthraquinone from cassiae semen, ameliorates lung inflammatory responses. Phytother Res 32: 1537-1545, 2018.
39. Lin S, Zhang Y, Wang Z, Zhang S, Li Y, Fan Y, Li D, Li S and Bai Y: Preparation of novel anthraquinone-based aspirin derivatives with anti-cancer activity. Eur J Pharmacol 900: 174020, 2021.
40. Zhou F, Ding M, Gu Y, Fan G, Liu C, Li Y, Sun R, Wu J, Li J, Xue X, *et al*: Aurantio-obtusin attenuates non-alcoholic fatty liver disease through AMPK-mediated autophagy and fatty acid oxidation pathways. Front Pharmacol 12: 826628, 2022.
41. Liu Y, Sun X, Hu X, Xu Y, Li T and Wu Z: Pharmacological properties and underlying mechanisms of aurantio-obtusin (review). Exp Ther Med 26: 380, 2023.
42. Li YJ, Wu RY, Liu RP, Wu KY, Ding MN, Sun R, Gu YQ, Zhou F, Wu JZ, Zheng Q, *et al*: Aurantio-obtusin ameliorates obesity by activating PPARα-dependent mitochondrial thermogenesis in brown adipose tissues. Acta Pharmacol Sin 44: 1826-1840, 2023.
43. Hu M, Zhong Y, Liu J, Zheng S, Lin L, Lin X, Liang B, Huang Y, Xian H, Li Z, *et al*: An adverse outcome pathway-based approach to assess aurantio-obtusin-induced hepatotoxicity. Toxicology 478: 153293, 2022.
44. Chandrashekar DS, Karthikeyan SK, Korla PK, Patel H, Shovon AR, Athar M, Netto GJ, Qin ZS, Kumar S, Manne U, *et al*: UALCAN: An update to the integrated cancer data analysis platform. Neoplasia 25: 18-27, 2022.
45. Gu L, Zhu Y, Lin X, Tan X, Lu B and Li Y: Stabilization of FASN by ACAT1-mediated GNPAT acetylation promotes lipid metabolism and hepatocarcinogenesis. Oncogene 39: 2437-2449, 2020.
46. Oh JM and Chun S: Ginsenoside CK inhibits the early stage of adipogenesis via the AMPK, MAPK, and AKT signaling pathways. Antioxidants (Basel) 11: 1890, 2022.
47. Yang R, Gao W, Wang Z, Jian H, Peng L, Yu X, Xue P, Peng W, Li K and Zeng P: Polyphyllin I induced ferroptosis to suppress the progression of hepatocellular carcinoma through activation of the mitochondrial dysfunction via Nrf2/HO-1/GPX4 axis. Phytomedicine 122: 155135, 2024.
48. Yamashita T, Honda M, Takatori H, Nishino R, Minato H, Takamura H, Ohta T and Kaneko S: Activation of lipogenic pathway correlates with cell proliferation and poor prognosis in hepatocellular carcinoma. J Hepatol 50: 100-110, 2009.
49. Zhou Y, Tao J, Calvisi DF and Chen X: Role of lipogenesis rewiring in hepatocellular carcinoma. Semin Liver Dis 42: 77-86, 2022.
50. Li S, Liu R, Pan Q, Wang G, Cheng D, Yang J, Chen H and Xu G: De novo lipogenesis is elicited dramatically in human hepatocellular carcinoma especially in hepatitis C virus-induced hepatocellular carcinoma. MedComm (2020) 1: 178-187, 2020.
51. Ma MKF, Lau EYT, Leung DHW, Lo J, Ho NPY, Cheng LKW, Ma S, Lin CH, Copland JA, Ding J, *et al*: Stearoyl-CoA desaturase regulates sorafenib resistance via modulation of ER stress-induced differentiation. J Hepatol 67: 979-990, 2017.
52. Muir K, Hazim A, He Y, Peyressatre M, Kim DY, Song X and Beretta L: Proteomic and lipidomic signatures of lipid metabolism in NASH-associated hepatocellular carcinoma. Cancer Res 73: 4722-4731, 2013.
53. Liu G, Kuang S, Cao R, Wang J, Peng Q and Sun C: Sorafenib kills liver cancer cells by disrupting SCD1-mediated synthesis of monounsaturated fatty acids via the ATP-AMPK-mTOR-SREBP1 signaling pathway. FASEB J 33: 10089-10103, 2019.
54. Igal RA: Stearoyl-CoA desaturase-1: A novel key player in the mechanisms of cell proliferation, programmed cell death and transformation to cancer. Carcinogenesis 31: 1509-1515, 2010.
55. Li L, Wang C, Calvisi DF, Evert M, Pilo MG, Jiang L, Yuneva M and Chen X: SCD1 expression is dispensable for hepatocarcinogenesis induced by AKT and Ras oncogenes in Mice. PLoS One 8: e75104, 2013.
56. Zhao Y, Li M, Yao X, Fei Y, Lin Z, Li Z, Cai K, Zhao Y and Luo Z: HCAR1/MCT1 regulates tumor ferroptosis through the lactate-mediated AMPK-SCD1 activity and its therapeutic implications. Cell Rep 33: 108487, 2020.
57. Wang Y, Wu X, Ren Z, Li Y, Zou W, Chen J and Wang H: Overcoming cancer chemotherapy resistance by the induction of ferroptosis. Drug Resist Updat 66: 100916, 2023.
58. Yi J, Zhu J, Wu J, Thompson CB and Jiang X: Oncogenic activation of PI3K-AKT-mTOR signaling suppresses ferroptosis via SREBP-mediated lipogenesis. Proc Natl Acad Sci USA 117: 31189-31197, 2020.
59. Tibori K, Orosz G, Zámbó V, Szelényi P, Sarnyai F, Tamási V, Rónai Z, Mátyási J, Tóth B, Csala M and Kereszturi É: Molecular mechanisms underlying the elevated expression of a potentially type 2 diabetes mellitus associated SCD1 variant. Int J Mol Sci 23: 6221, 2022.
60. Martín-Núñez GM, Cabrera-Mulero R, Rojo-Martínez G, Gómez-Zumaquero JM, Chaves FJ, de Marco G, Soriguer F, Castaño L and Morcillo S: Polymorphisms in the SCD1 gene are associated with indices of stearoyl CoA desaturase activity and obesity: A prospective study. Mol Nutr Food Res 57: 2177-2184, 2013.
61. Zhou J, Zhang L, Yan J, Hou A, Sui W and Sun M: Curcumin induces ferroptosis in A549 CD133$^+$ cells through the GSH-GPX4 and FSP1-CoQ10-NAPH pathways. Discov Med 35: 251-263, 2023.
62. Xie Y, Kang R, Klionsky DJ and Tang D: GPX4 in cell death, autophagy, and disease. Autophagy 19: 2621-2638, 2023.
63. Wang H, Wang C, Li B, Zheng C, Liu G, Liu Z, Zhang L and Xu P: Discovery of ML210-based glutathione peroxidase 4 (GPX4) degrader inducing ferroptosis of human cancer cells. Eur J Med Chem 254: 115343, 2023.
64. Wang Q, Bin C, Xue Q, Gao Q, Huang A, Wang K and Tang N: GSTZ1 sensitizes hepatocellular carcinoma cells to sorafenib-induced ferroptosis via inhibition of NRF2/GPX4 axis. Cell Death Dis 12: 426, 2021.
65. Xuan Y, Wang H, Yung MM, Chen F, Chan WS, Chan YS, Tsui SK, Ngan HY, Chan KK and Chan DW: SCD1/FADS2 fatty acid desaturases equipoise lipid metabolic activity and redox-driven ferroptosis in ascites-derived ovarian cancer cells. Theranostics 12: 3534-3552, 2022.